Title

Initial scaffold thickness affects the emergence of a geometrical and mechanical equilibrium in engineered cardiovascular tissues.

Journal

Journal of the Royal Society Interface, 15(148)

Authors

van Kelle, M

Oomen, Pim

Janssen-van den Broek, W

et al.

Publication Date

2018-11-14

DOI

10.1098/rsif.2018.0359

Peer reviewed

INTERFACE

rsif.royalsocietypublishing.org

Research

Cite this article: van Kelle MAJ, Oomen PJA, Janssen-van den Broek WJT, Lopata RGP, Loerakker S, Bouten CVC. 2018 Initial scaffold thickness affects the emergence of a geometrical and mechanical equilibrium in engineered cardiovascular tissues. *J. R. Soc. Interface* **15**: 20180359.
http://dx.doi.org/10.1098/rsif.2018.0359

Received: 18 May 2018
Accepted: 16 October 2018

Subject Category:
Life Sciences–Engineering interface

Subject Areas:
biomedical engineering, biomechanics, bioengineering

Keywords:
cardiovascular, tissue-engineering, growth, remodelling

Author for correspondence:
S. Loerakker
e-mail: s.loerakker@tue.nl

†These authors contributed equally to this study.
‡Shared last authors.

Electronic supplementary material is available online at https://dx.doi.org/10.6084/m9.figshare.c.4285721.

THE ROYAL SOCIETY PUBLISHING

Initial scaffold thickness affects the emergence of a geometrical and mechanical equilibrium in engineered cardiovascular tissues

M. A. J. van Kelle[1,2,†], P. J. A. Oomen[1,2,†], W. J. T. Janssen-van den Broek[1,2], R. G. P. Lopata[1], S. Loerakker[1,2,‡] and C. V. C. Bouten[1,2,‡]

[1]Department of Biomedical Engineering, and [2]Institute for Complex Molecular Systems, Eindhoven University of Technology, Eindhoven, The Netherlands

MAJvK, 0000-0003-0768-513X; PJAO, 0000-0002-0069-4538; RGPL, 0000-0001-6618-6184; SL, 0000-0002-9574-1623; CVCB, 0000-0003-1035-5094

In situ cardiovascular tissue-engineering can potentially address the shortcomings of the current replacement therapies, in particular, their inability to grow and remodel. In native tissues, it is widely accepted that physiological growth and remodelling occur to maintain a homeostatic mechanical state to conserve its function, regardless of changes in the mechanical environment. A similar homeostatic state should be reached for tissue-engineered (TE) prostheses to ensure proper functioning. For *in situ* tissue-engineering approaches obtaining such a state greatly relies on the initial scaffold design parameters. In this study, it is investigated if the simple scaffold design parameter initial thickness, influences the emergence of a mechanical and geometrical equilibrium state in *in vitro* TE constructs, which resemble thin cardiovascular tissues such as heart valves and arteries. Towards this end, two sample groups with different initial thicknesses of myofibroblast-seeded polycaprolactone-bisurea constructs were cultured for three weeks under dynamic loading conditions, while tracking geometrical and mechanical changes temporally using non-destructive ultrasound imaging. A mechanical equilibrium was reached in both groups, although at different magnitudes of the investigated mechanical quantities. Interestingly, a geometrically stable state was only established in the thicker constructs, while the thinner constructs' length continuously increased. This demonstrates that reaching geometrical and mechanical stability in TE constructs is highly dependent on functional scaffold design.

1. Introduction

Cardiovascular diseases remain the leading cause of death worldwide. If the many therapies that are available to alleviate, or slow down these diseases, fail, prostheses are available to replace end-stage diseased cardiovascular tissues. Autologous, bioprosthetic and synthetic prostheses are widely used for replacing diseased arteries and heart valves, yet repetitive surgery is often required owing to postoperative complications such as calcification, infection and aneurysm formation [1–5]. Moreover, the lack of growth and remodelling capacity of artificial prostheses may necessitate multiple re-operations for paediatric patients [6,7], resulting in a lower life expectancy and quality of life [8].

Tissue engineering can potentially address the shortcomings of current cardiovascular tissue replacements, in particular, their inability to grow and remodel. Tissue engineering aims to create autologous tissue replacements from biodegradable materials [9,10]. Previous studies have already shown that tissue-engineered (TE) vessels and heart valves prostheses have the potential for growth and remodelling. For instance, Hoerstrup *et al.* [11] implanted

TE vascular grafts in the pulmonary artery of a growing lamb. While the animal's weight increased twofold during a 2-year follow-up period, the graft diameter (30%) and length (45%) increased significantly. More recently, a similar animal model was used to demonstrate that decellularized vascular grafts show a similar trend, with the diameter increasing 56% upon a 366% increase in animal body weight. Neo-tissue formation was found in all of the explanted grafts [12], thus eliminating dilation as the only cause of increased diameter. Finally, Kluin *et al.* obtained a fully functional TE heart valve with mature and stable tissue formation after 12 months, using an *in situ* implanted, slow-degrading scaffold [13].

To date, our understanding of growth and remodelling in engineered tissues remains incomplete. In native tissues, physiological growth and remodelling is widely believed to occur in order to maintain a certain homeostatic mechanical state [14–17]. Through this principle, tissues can maintain their function regardless of changes in their mechanical environment. Several mechanical quantities have been proposed to determine mechanical homeostasis across different cardiovascular native tissues, including stretch [18,19], stress [20–22], strain energy density [23,24] and stiffness [25,26].

Interestingly, it appears that in previous studies no mechanical homeostasis may have been established in TE prostheses. On the contrary, despite promising early results, adverse growth and remodelling of TE prostheses have led to geometrical instabilities, i.e. aneurysm formation in TE vascular grafts [27–29], and leaflet shortening in TE heart valves that causes valvular insufficiency [30–32]. We believe that the scaffold design of (*in situ*) TE prostheses is crucial to obtain and maintain mechanical and geometrical homeostasis. Many design parameters can be tuned when producing scaffolds for tissue engineering, for instance: scaffold thickness, porosity, fibre alignment, fibre diameter, compliance, degradation rate and polymer composition. All of these parameters influence the mechanical properties of scaffolds, and can therefore influence growth and remodelling and subsequently the establishment of homeostasis. Previously, both *in vivo* [33] and *in silico* [34] models have been used to assess the influence of scaffold properties on growth and remodelling in TE prostheses. Most recently, Best *et al.* [35] clearly demonstrated in an *in vivo* study that decreasing the scaffold thickness to diameter ratio positively affects long-term growth and remodelling of TE vascular grafts.

In the current study, we aim to determine and understand the effects of initial scaffold thickness on establishing a geometrical and mechanical equilibrium in thin engineered cardiovascular tissues, such as heart valves and arteries. To this end, a recently developed *in vitro* bioreactor [36] was used to culture two groups of TE cardiovascular constructs with different initial thicknesses (relevant for cardiovascular tissue engineering), under the same dynamic loading conditions. In order to investigate whether geometrical and/or mechanical equilibrium was established in the TE constructs, temporal changes in tissue geometry and mechanical state were quantified at several time points during development, by means of non-destructive ultrasound imaging and inverse analysis [37]. At the end of culture, the TE constructs' composition and structure were determined by biochemical assays, histology and in-plane collagen organization.

It was found that a mechanical steady state was reached for both sample thicknesses, although at different magnitudes of the investigated mechanical quantities (strain, stress, strain energy density and tangent). A stable geometrical state was only reached in the thicker samples, while the thinner constructs continued to elongate. These results indicate that obtaining a geometrically and mechanically stable state in TE constructs is highly dependent on functional scaffold design, in this particular case the initial scaffold thickness.

2. Methods

2.1. Scaffold production

Two supramolecular scaffold sheets with respective thicknesses of 0.31 ± 0.01 and 0.47 ± 0.01 mm were produced in-house via electrospinning. Polycaprolactone-bisurea (PCL-bu) polymer [38] (SyMO-Chem, Eindhoven, The Netherlands) was dissolved in chloroform to a 15 wt% concentration and electrospun in a climate-controlled electrospinning cabinet (IME Technology, Geldrop, The Netherlands). The cabinet was equipped with a 14G nozzle (flow rate of 55 µl min $^{-1}$) and a distance of 16 cm was maintained between nozzle and the grounded target drum (0.31×12.0 cm), rotating at 100 r.p.m. The climate chamber was set to 23°C, 30% relative humidity and a voltage of 15 kV was applied to the nozzle. After spinning, the two sheets were dried overnight under vacuum at room temperature. Each sheet was inspected with scanning electron microscopy. Additionally, the thicknesses of the sheets were assessed using a VHX-500 Keyence digital microscope.

2.2. Scaffold mechanical (fatigue) testing

Fatigue tests were performed on the bare scaffold materials, using an ElectroForce LM1 TestBench by BOSE equipped with 5 N load cells. Two rectangular samples (15×6.5 mm) were cut from each sheet, which were uniaxially stretched for 1.8 million cycles (equal to 21 days of dynamic culturing, see §2.3) with increasing maximum actuator displacements of 5, 10, 15 and 20% of the initial sample length. Every displacement stage consisted of two periods of 225 000 sinusoid displacement cycles at 10 Hz, each followed by a rest period of equal duration to cyclic displacement (22 500 s). During testing, the samples were submerged in a physiological salt solution at 37°C. From this test, the peak first Piola–Kirchhoff stresses were calculated from the force acting on the load cells as a function of time.

Uniaxial tensile tests of the scaffolds were performed before and after fatigue testing on a BioTester (CellScale, Waterloo, Canada). The samples were stretched to 115% of the initial length with a strain rate of 100% min^{-1} for 10 cycles, of which the first nine were considered pre-conditioning. During testing, the samples were again submerged in a physiological salt solution at 37°C. The force was measured by a 1.5 N load cell, and images were taken by a CCD camera mounted perpendicular to the sample surface. All data were collected with a sampling frequency of 5 Hz. Again the first Piola–Kirchhoff stresses were calculated from the force data. The in-plane sample stretches were obtained from the images using a global digital image correlation algorithm [39].

2.3. Tissue culture in bioreactor

To culture TE constructs, the versatile tissue growth and remodelling (Vertigro) bioreactor [36] was used (figure 1). Inside this bioreactor a circular insert with a diameter of 15 mm containing a cell-seeded construct can be placed which is then consecutively cultured under pressure-driven dynamic loading conditions. Regardless of geometrical and mechanical changes in the construct, the applied pressures were maintained by a custom LabView (National Instruments, Austin, USA) program.

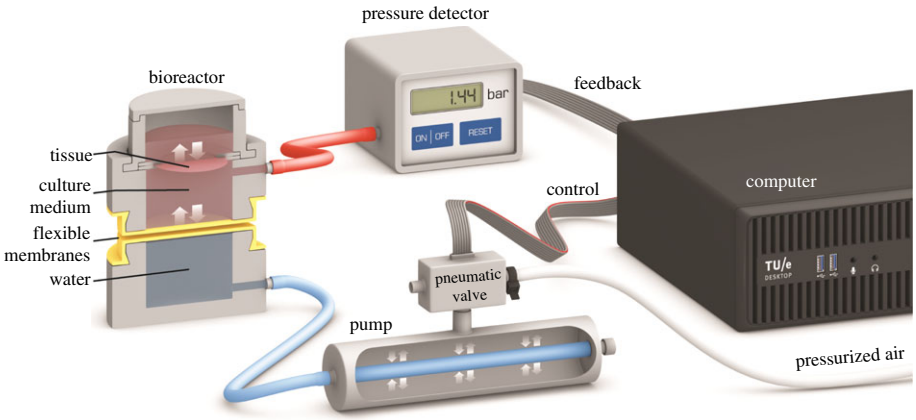

Figure 1. Schematic of the Vertigro bioreactor and pressure application system. Source: van Kelle *et al.* [36], Copyright: Mary Ann Liebert, granted permission for reprint.

The electrospun PCL-bu scaffolds (§2.1) (both $n = 8$) were clamped in the inserts and sterilized using ultraviolet light. Next, 0.25 mg ml^{-1} L-ascorbic 2-phosphate acid (Sigma-Aldrich, St Louis, MO, USA) supplemented standard culture medium (TE medium) was added to the inserts after which they were placed in an incubator overnight. Primary myofibroblast-like cells were isolated from human vena saphena samples, according to the Dutch guidelines for use of secondary materials. These cells exhibit a contractile phenotype, and are known to produce abundant amounts of extracellular matrix [40], making them ideal for cardiovascular tissue engineering. The cells were cultured in advanced Dulbecco's modified Eagle medium (Invitrogen, Carlsbac, CA, USA), supplemented with 10% fetal bovine serum (Greiner Bio One, Frinckenhausen, Germany), 1% Glutamax (Invitrogen) and 1% penicillin/streptomycin (Lonza, Basel, Switzerland) which was changed twice per week. At passage 7, the cells were harvested and seeded on the PCL-bu scaffolds using a seeding density of 15 million cells cm^{-3} using fibrin as a cell carrier [41]. After seeding, TE medium was added to the constructs which were then statically cultured at 37°C, 100% humidity and 5% CO_2 to allow for initial tissue development. After this period, the inserts containing the constructs were placed in the bioreactor and cultured for 21 days at a dynamic loading regime with a maximum pressure of 4 kPa at 1 Hz.

2.4. Non-destructive geometrical and mechanical characterization during culture

Changes in tissue geometry and mechanical state were nondestructively characterized at day 0, 3, 7, 14 and 21 of dynamic culturing. At each time point, a 12 MHz linear ultrasound transducer (LA435) connected to a MyLab 70 Ultrasound system (Esaote Europe, Maastricht, The Netherlands) was positioned on top of the bioreactor, perpendicular to the construct surface and aligned with the centre of the construct. The transducer was positioned at the same location as during previous measurements. To prevent infections during culture, the measurements were performed inside a laminar air flow cabinet, with the ultrasound probe contained in a sterile probe cover (Civco, Coralville, IA, USA). To assess the construct thickness, raw radio-frequency data were acquired without applying any pressure. From these data, the thickness was determined in approximately 20 locations using MATLAB's (Mathworks, Natick, MA, USA) *findpeaks* algorithm, of which the median thickness was used as initial construct thickness t_0.

Next, a mechanical test was performed during which a pressure (p) of 4 kPa (the same maximal pressure used during dynamic culturing) was gradually applied to the constructs, while imaging the constructs' deformation with the ultrasound scanner. Three pressure cycles were applied in each test, of which the first two were considered as preconditioning. The pressure was measured by a pressure sensor (P10EZ-1, BD—SENSORS, Thierstein, Germany). The constructs' geometries were assumed to be axi-symmetric and their mechanical properties isotropic, hence one measurement in any given direction was assumed to be representative for all other directions.

The sample profile as a function of pressure was tracked in the B-mode images (frame rate 25 Hz, resolution 21 px mm^{-1}) using a custom MATLAB script [37]. First, the two attachment points of the constructs were selected after which for each frame the tissue apex was manually selected. A circle was subsequently fitted through the attachment points and the apex to describe the tissue profile. This profile was used to calculate the construct curvature k and current length L. The unloaded construct length L_0 was defined at $p = 0$, and the construct stretch during pressure application as $\lambda = L/L_0$.

2.5. Mechanical properties and mechanical state during culture

2.5.1. Constitutive model

The material behaviour of the TE constructs was modelled by a hyperelastic fibre-reinforced constitutive model, where the Cauchy stress σ was obtained from a strain energy density function Ψ as a function of a set of material parameters ξ:

$$\boldsymbol{\sigma} = \frac{2}{J}\mathbf{F}\cdot\frac{\partial \Psi(\xi)}{\partial \mathbf{C}}\cdot\mathbf{F}^{\mathrm{T}}, \tag{2.1}$$

with $\mathbf{F}$ the deformation gradient tensor, $\mathbf{C} = \mathbf{F}^{\mathrm{T}}\cdot\mathbf{F}$ the right Cauchy–Green deformation tensor and $J = \det(\mathbf{F})$ the Jacobian. The strain energy density function consisted of an isotropic matrix part m and anisotropic fibrous part f with fibre volume fraction Φ_f, arbitrarily set at 0.5 [42]:

$$\Psi = (1 - \Phi_f)\Psi_m + \Phi_f\Psi_f. \tag{2.2}$$

The constitutive behaviour of the isotropic matrix part was described by a Neo-Hookean constitutive model:

$$\Psi_m = \frac{\kappa}{2}\ln^2(J) + \frac{\mu}{2}(I_1 - 3 - 2\ln(J)), \tag{2.3}$$

where $\kappa = 2\mu(1+\nu)/3(1-2\nu)$ is the bulk modulus, μ the shear modulus, and $I_1 = \mathbf{C}:\mathbf{I}$ the first invariant of the right Cauchy–Green deformation tensor. Quasi-incompressibility was enforced by setting the Poisson ratio at $\nu = 0.498$. The fibre part was modelled as an isotropic discrete fibre distribution oriented in the plane of the sample (as was also

evident from the histological and microscopic analyses of the constructs). Each fibre i with unit direction vector $\mathbf{e}_f^i$ (in the reference configuration) additively contributed [42] to the total fibre strain energy density function Ψ_f. The strain energy density function Ψ_f^i for each individual fibre i was given by an exponential model (similar to [42–44]):

$$\Psi_f^i = \frac{k_1}{2k_2}(\exp[k_2\langle(\lambda^i)^2 - 1\rangle] - k_2\langle(\lambda^i)^2 - 1\rangle - 1), \tag{2.4}$$

with k_1 and k_2 material parameters, $(\lambda^i)^2 = \mathbf{C}{:}(\mathbf{e}_f^i \otimes \mathbf{e}_f^i)$ the squared elastic fibre stretch, and $\langle^\circ\rangle$ the Macaulay brackets to enforce that the fibres only resist tension. The ability of this constitutive model to adequately describe the mechanical behaviour of TE constructs was previously demonstrated [37].

2.5.2. Estimation of material properties

From each nondestructive mechanical test, the construct's profile as a function of pressure was recorded at each time point. Using this information, the material properties ξ (here $\xi = [\mu, k_1, k_2]$) of the constructs at each time point were determined using a two-step inverse method that was previously developed [37]. In the first step, shell theory was used to obtain a rapid analytical estimate of the material properties. This estimate was used as an initial estimate of the second step, where an inverse finite-element analysis was used to obtain a more accurate estimate of the material properties. In this step, the experiments were simulated by a finite-element model in Abaqus FEA (Dassault Systèmes Simulia Corp., Providence, RI, USA). Only one quarter of the tissue geometry (at $p = 0$) was modelled owing to symmetry. A uniform pressure was applied to the bottom plane of the construct, while the nodes on the sample edge were fully constrained. MATLAB's *lsqnonlin* function was used to adjust the material parameter set ξ until the difference between the surface profile as a function of pressure $z(p)$ between the experiment (exp) and the estimate (est) was minimized. This resulted in the following cost function:

$$E(\xi) = \frac{1}{N_p N_x}\sum_{j=1}^{N_p}\sum_{k=1}^{N_x}\sqrt{z(p_j, x_k, \xi)^{\text{exp}} - z(p_j, x_k, \xi)^{\text{est}}}, \tag{2.5}$$

with N_p the number or pressure steps, N_x the number of in-plane positions x along the tissue profile.

2.5.3. Analysis of the mechanical state

After the material parameter estimation, the strain energy density, the Cauchy stress tensor and deformation gradient tensor at every node in the central 50% of the construct were obtained from the final simulation of the inverse finite-element analysis. Subsequently, the maximum principal stress $\sigma_{\max}$ and its direction $\mathbf{n}_{\max}$ were determined. The stretch $\lambda_{\max}$ in the same direction $\mathbf{n}_{\max}$ was then obtained from $\lambda_{\max} = 1/\sqrt{\mathbf{B}^{-1}{:}(\mathbf{n}_{\max} \otimes \mathbf{n}_{\max})}$, with $\mathbf{B}$ the left Cauchy–Green deformation tensor. The local tangent of the principal stress–stretch curve was determined at $p = 4$ kPa.

2.6. Tissue analysis after culture

After culture (day 21 of dynamic culture), the constructs were cut into three pieces. Two quarters were fixed in 3.7% formaldehyde and used for histology and collagen orientation analysis, respectively. The other half of the samples were lyophilized overnight and used to quantify the amounts of DNA, glycosaminoglycans (GAGs) and hydroxyproline (HYP; as measure for the amount of collagen).

From each sample, the first quarter was embedded in paraffin and sectioned into slices of 7 µm. The embedded samples were stained for general tissue structure (hematoxylin & eosin (HE)), collagen (picrosirius red (PR)) and GAGs (safranin O (SO)). These sections were imaged under a brightfield microscope (Axio Observer Z1, Carl Zeiss AG, Oberkochen, Germany), and the PR stain was also imaged using polarized light. In addition, fluorescent stainings were performed for collagen type III, (Tropo)elastin and a costaining for collagen type 1, α-smooth muscle actin (α-SMA) and cell nuclei, which all were imaged using an Axiovert 200M microscope (Zeiss).

The other quarter of the samples was incubated with a collagen-specific CNA35 [45] probe for 1 h, after which the gross collagen organization was imaged via a tilescan on each side (excitation 488 nm, emission 520 nm, magnification 10 ×) using a confocal laser scanning microscope (TCS SP5X; Leica Microsystems, Wetzlar, Germany). To quantify the in-plane collagen fibre organization, a custom-made MATLAB script was used [46], which quantifies the fraction of fibres oriented in each in-plane direction.

Finally, the lyophilized halves of the constructs were snap-frozen and disintegrated using a Mikro-Dismembrator (Model S, Sartorius, Goettingen, Germany), followed by digestion using a papain digestion buffer (60°C, 16 h). The constructs' total GAG content were determined using an adapted protocol by Farndale *et al.* [47], with a standard curve of chondroitin sulfate (Shark Cartilage, Sigma-Aldrich). An HYP assay was performed [48] using a trans-4-hydroxyproline (Sigma-Aldrich) standard curve. To obtain a measure for cellular activity, construct GAG and HYP content were normalized to the tissue's total DNA content, which was determined with the Hoechst dye method [49].

2.7. Statistics and sample numbers

During the experiment, unfortunately a few samples were excluded owing to an infection. For the thin samples, one sample was excluded during the second week, and two samples in the final week of dynamic culture. For the thick samples, in both the second and final week one sample was excluded. Consequently, all analyses at the end of the experiment were performed with $n = 5$ and $n = 6$ samples for the thin and thick group, respectively. The geometrical and mechanical measurements of samples before drop-out were still taken into account. All data are presented as mean value $\pm$ the standard error of the mean. For the biochemical assay data, comparisons between groups were made using the Wilcoxon signed-rank statistical test in MATLAB. The geometrical and mechanical data were analysed in IBM SPSS Statistics for Macintosh (IBM Corp., Armonk, NY, USA), using linear mixed model analysis, according to Duricki *et al.* [50]. This is a statistical approach that accounts for multiple measurements in the same (in this case) constructs, while accommodating for possible dropout of samples during the experiment. Post hoc analyses using Fisher's least significant difference tests were used to test for statistical different between adjacent time points within each initial construct thickness group, and between the two groups at the same time point. Differences were considered statistically different when $p < 0.05$.

3. Results

3.1. Geometrical changes during culture

The geometrical changes of the tissue constructs are depicted in figure 2. Initially, both groups started with a tissue length L_0 of 15 mm (in accordance with the diameter of the bioreactor insert; figure 2*a*). However, after only 3 days of dynamic culturing the samples both elongated significantly, where the length of the thinner samples was larger than that of the thicker samples. This trend continued over time for the

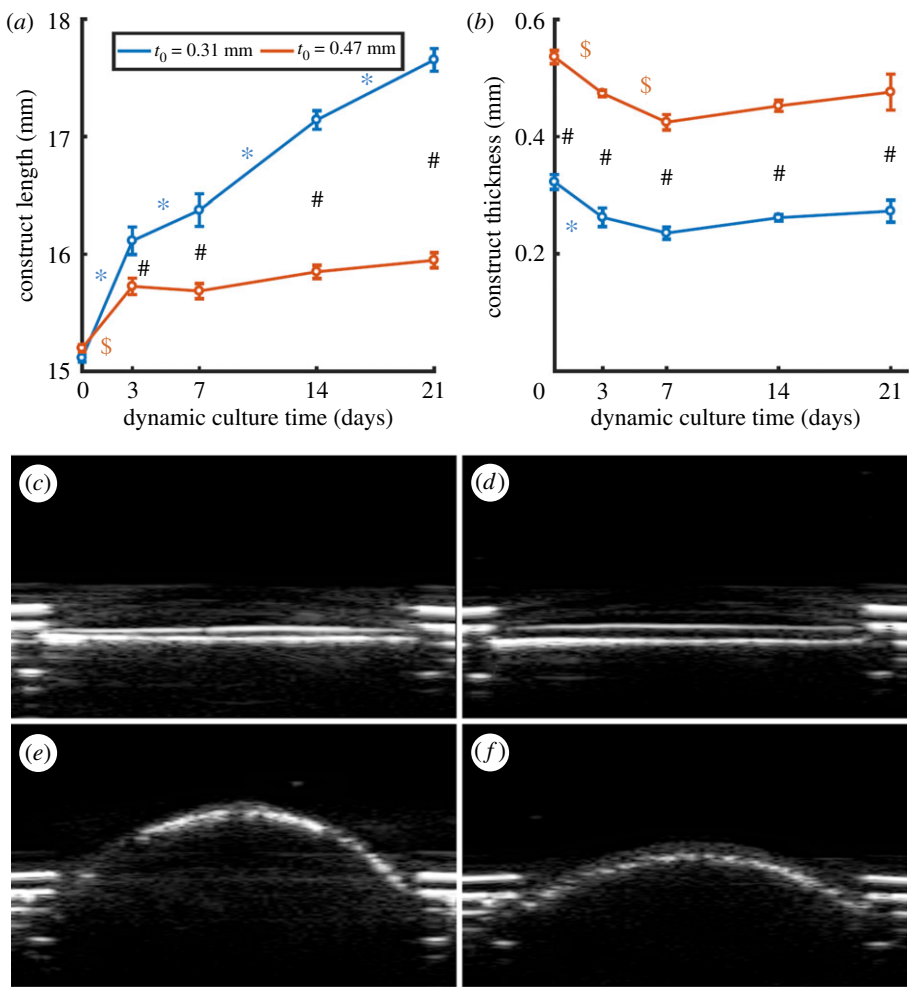

Figure 2. Geometrical changes of the constructs during dynamic culture: changes in tissue length L_0 (*a*) and construct thickness t_0 (*b*) for starting scaffold thicknesses of 0.31 mm (blue) and 0.47 mm (red). Significant changes ($p < 0.05$) between adjacent time points within the initially thinner and thicker constructs are indicated by * and $, respectively, while significant differences between the two groups at the same time point are indicated by #. Representative ultrasound images (with $p = 0$) of the thin (*c*,*e*) and thick (*d*,*f*) constructs at the start (*c*,*d*) and end (*e*,*f*) of the dynamic culturing.

initially thinner tissues, while the thicker construct length did not significantly change with time. At the end of culture, the length of the tissues of both groups had significantly increased (figure 2*e*,*f*) compared to the start of culture (figure 2*c*,*d*). The construct thickness t_0 at the start of the dynamic culturing phase was similar to the initial scaffold thickness (figure 2*b*). Next, both groups followed a similar trend, where first a significant decrease in thickness was observed up to day 7, after which the thickness slightly increased again up to day 21.

3.2. Construct mechanics during culture

The material parameters of the engineered constructs were successfully estimated during dynamic culture (see the electronic supplementary material). From these material parameters, several mechanical constituents were quantified during dynamic culture in the central 50% of the constructs. The elastic stretch, maximum principal Cauchy stress, strain energy density and local tangent of the principal stress–stretch curve at $p = 4$ kPa in the thin constructs were higher than in the thick constructs (figure 3). During tissue development, the elastic stretch of the constructs in the two groups diverged towards significantly different equilibrium states, with the stretch in the thin constructs slightly increasing and the stretch in the thick constructs decreasing with time. The strain energy density stabilized during development, with no significant changes between adjacent time points observed during dynamic culture. The maximum principal Cauchy stress of the thin samples appeared to decrease with culture time, while the stress in the thicker samples increased up to day 7, followed by a decrease. Finally, the tangent in both groups appeared to decrease during development, albeit in the thick samples after an initial increase and with no significant changes between adjacent time points. No significant differences were found between the local tangents of the two groups after the start of dynamic culture.

3.3. Bare scaffold features progressive viscoelastic and plastic deformation

Fatigue tests were performed on both scaffold thicknesses, during which increasing actuator displacements were applied to stretch the scaffolds (figure 4*a*). During each actuator displacement stage, the peak first Piola–Kirchhoff stress decreased, which can be attributed to progressive plastic (permanent) length change of the scaffolds (figure 4*c*,*d*). After the rest period that was applied during each displacement stage, the stress only partially recovered to the same magnitude as found before the rest period. This indicates

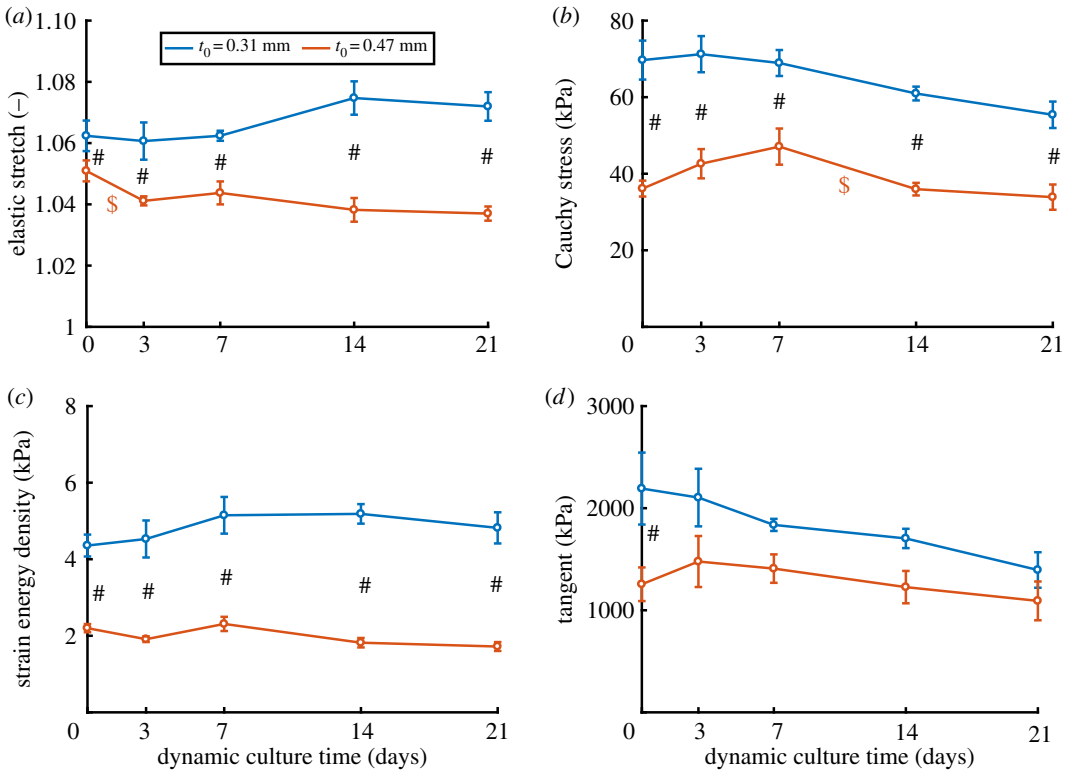

Figure 3. Assessment of the constructs' mechanical state during dynamic culture. In all constructs, the stretch (*a*), maximum principal Cauchy stress (*b*), strain energy density (*c*) and tangent of the principal stress–stretch curve at $p = 4$ kPa (*d*) were non-destructively quantified. Significant changes ($p < 0.05$) between adjacent time points within the initially thinner and thicker samples are indicated by * and $, respectively, while significant differences between the two groups at the same time point are indicated by #.

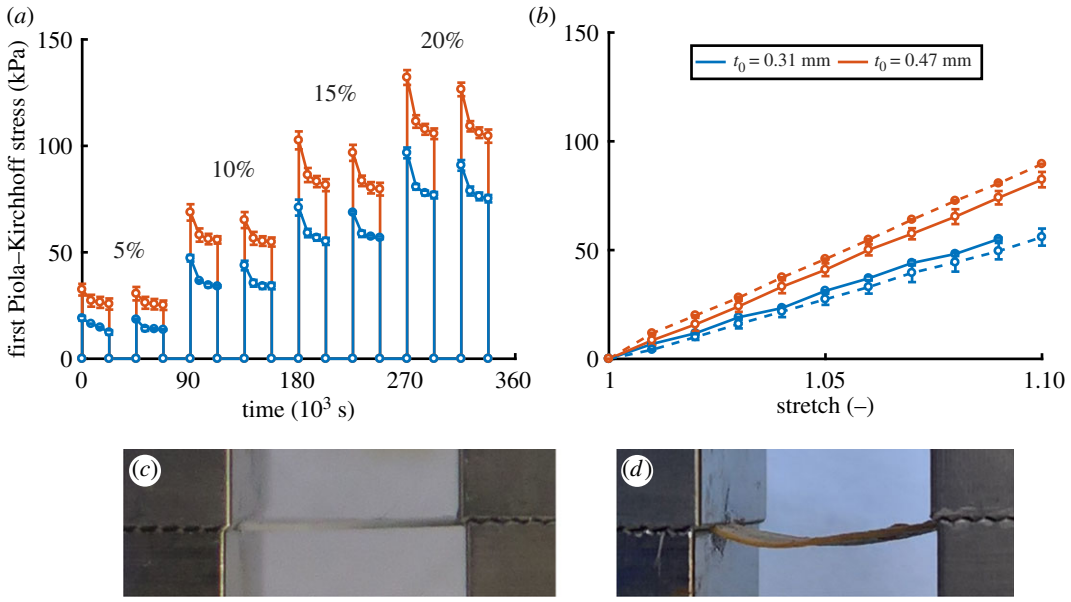

Figure 4. Mechanical testing of the bare scaffold. First Piola–Kirchhoff stress during fatigue testing with increasing actuator displacements (*a*). Images were captured before (*c*) and several hours after (*d*) fatigue testing, here shown for a sample of $t_0 = 0.31$ mm. The stress–stretch behaviour of each sample was characterized before (continuous lines) and after (dashed lines) fatigue testing (*b*).

that stress relaxation occurred during each stage, thus identifying the scaffolds as viscoelastic materials.

Despite the plastic deformation that occurred during fatigue testing, additional uniaxial tests performed before and after fatigue testing showed no clear differences in the mechanical behaviour of both scaffold groups (figure 4*b*). Both the fatigue and additional tensile tests indicated that the thin scaffolds were more compliant than the thick scaffolds.

3.4. Collagen formation occurs isotropically in-plane

An in-plane isotropically distributed collagen organization was observed on both sides of a quarter of the engineered constructs (figure 5). Using fibre tracking software, this was also confirmed quantitatively, as indicated in the histograms of figure 5. When comparing both sides of the samples, the top part has a more dense collagen fibre

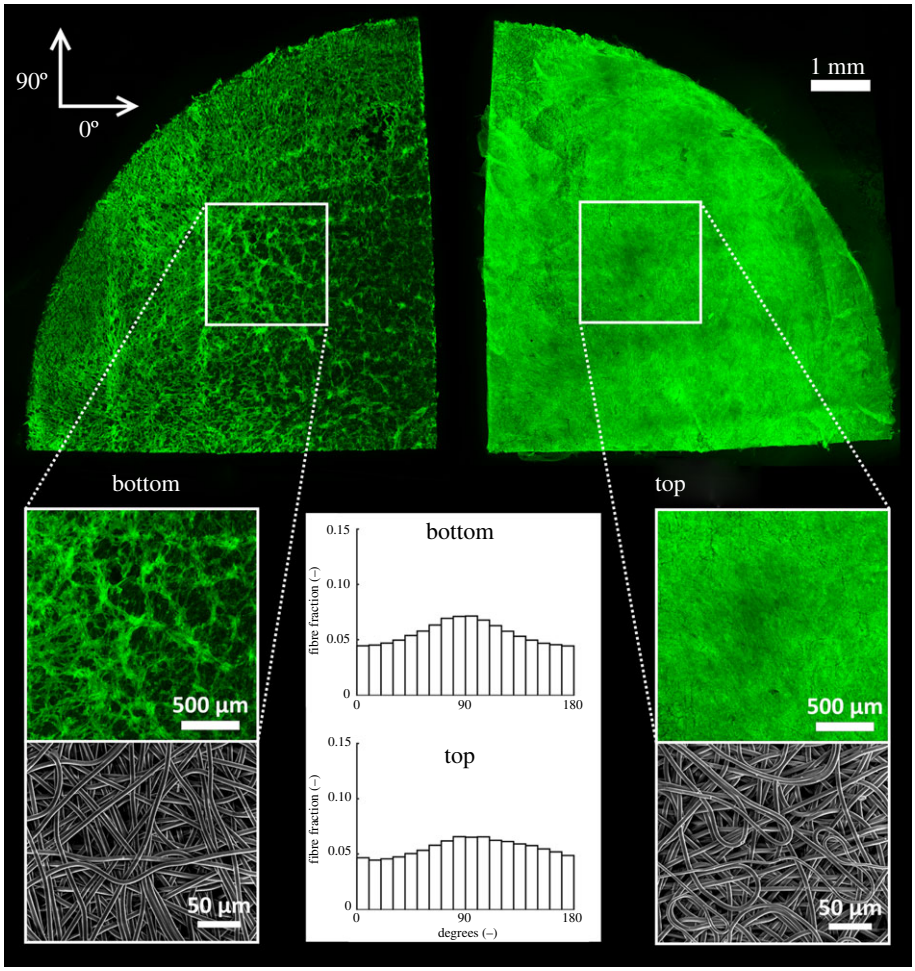

Figure 5. The top (right) and bottom (left) side of a representative collagen-stained quarter of one of the constructs. Zoomed-in images are indicated between the white squares, with below them scanning electron images of the scaffold prior to seeding. The histograms indicates the fraction of collagen fibres oriented in each direction for the entire sample.

network compared to the bottom part, which contains more thick bundles of fibres.

3.5. Layered tissue formation throughout the samples thickness

Figure 6 shows representative histological images for the thin (left column) and thick (right column) samples. Note that the scaffold was still present at the end of the experiment, but was dissolved owing to solvents used during the embedding process. The HE stain showed a more dense structural organization in the thick samples, compared to the thin samples (*a*,*b*). In addition, a distinct layer formation was present on the top side of both sample groups, which was also visible in the PR stain (*c*,*d*). When polarized light was used to asses the maturity of the fibres, the bright-red mature fibres were found opposite of this top layer at the pressurized sides of the samples. α-SMA-positive cells were mostly located in the top layer of the tissue, together with relatively immature collagen type III (*g*,*h*,*i*,*j*). On the other hand, some elastin fibres were present on the pressured sides of the samples (figure 6 *k*,*l*). Finally, GAGs were most abundant in the thicker samples, also evenly distributed throughout the thickness.

3.6. Increased GAG formation in thick constructs

Figure 7 shows the results for the biochemical assays performed on the lyophilized samples at the end of the experiment. The mean DNA content (microgram) for each group is slightly higher in the thicker samples (figure 7*a*), these values were used to normalize the total GAG and HYP content. The constructs' GAGs per DNA (figure 7*b*) content was significantly ($p = 0.03$) higher for the thick samples, while the opposite is true for the amount of HYP per DNA (figure 7*c*).

4. Discussion

This study sought to determine *in vitro* whether a geometrical and/or mechanical equilibrium state could be reached in engineered cardiovascular constructs depending on initial scaffold thickness. Towards this end, temporal changes in geometry and mechanical properties in dynamically cultured constructs were assessed over time using non-destructive ultrasound imaging.

4.1. Geometrical equilibrium is dependent on initial scaffold thickness

In the fatigue tests performed on the bare scaffold material (figure 4), both the thin and thick samples plastically deformed at all of the applied levels of actuator displacement. Moreover, the electrospun materials showed viscoelastic behaviour, as indicated by the increase in peak first Piola–Kirchoff stress after a period of rest. It should be noted that

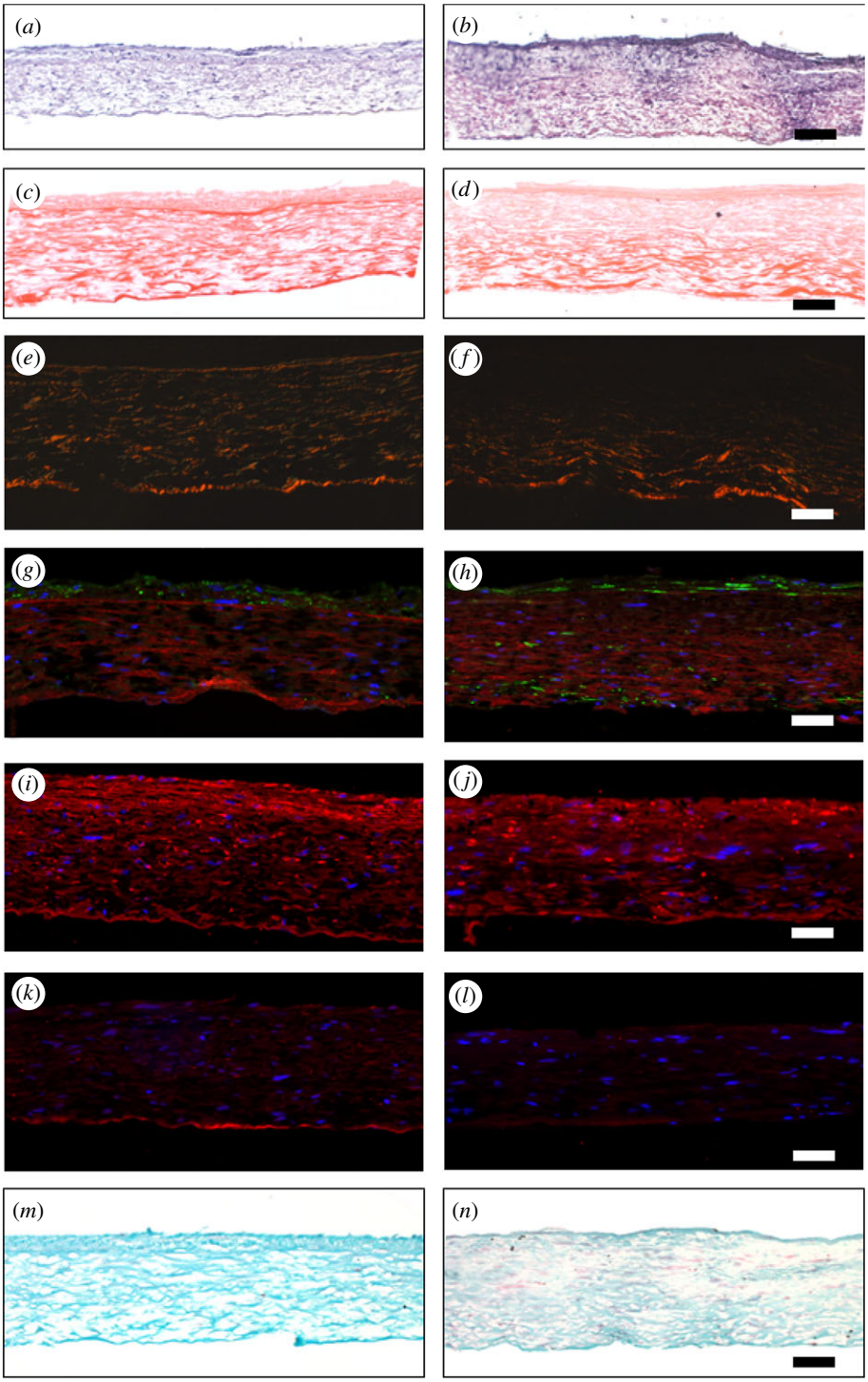

Figure 6. Representative histological images of the middle section for the thin (left column) and thick (right column) samples at $t = 21$ days of dynamic culture, where the bottom side of all samples coincides with the pressurized side in the bioreactor. (*a*,*b*) HE stain showing the general tissue composition, with a distinct layer formation on the top side of the samples. (*c*,*d*) PR stain showed general collagen organization (red). (*e*,*f*) PR stain visualized with polarized light, depicting relatively mature collagen fibres (red). (*g*,*h*) Fluorescent images with α-SMA-positive cells in green, cell nuclei in blue and collagen in red. (*i*,*j*) Fluorescent stain for collagen type III. (*k*,*l*) Co-fluorescent stain for elastin (red) and cell nuclei (blue). (*m*,*n*) SO stain depicting GAGs in red. The scale of the images is indicated by the black and white bars (100 µm) (HE, hematoxylin & eosin; PR, picosirius red; SO, safarin O).

both permanent deformation and viscoelastic behaviour will probably have the same lengthening effects *in vivo*, as in this case the material will never experience an unloaded state.

The cell-seeded scaffolds experienced a similar type of dynamic loading compared to the bare scaffolds, during which lengthening of the sample was compensated by the feedback system of the bioreactor, in order to maintain a constant peak pressure. As with the bare scaffolds, construct length increased during dynamic culture, and was dependent on the initial scaffold thickness (figure 2). Strikingly, the initially thin construct length continued to increase, whereas the thicker constructs length stabilized after 3 days of dynamic culture. In the thin samples, this apparently causes the tissue length to continue dilating, whereas the thicker samples are able to counteract this lengthening. A possible explanation could be attributed to the fact that there is more extracellular matrix (ECM) production in the thick samples, in the form of cell-produced GAGs (figure 7). Moreover, a more dense collagen structure was observed in the thicker samples (figure 6*g*,*h*), which could also explain

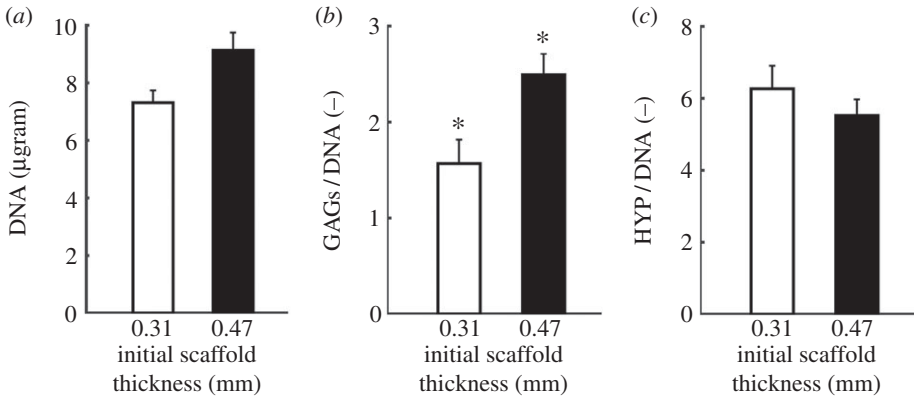

Figure 7. Biochemical assays: total DNA content (μgram) (*a*) GAGs per DNA (*b*) and HYP per DNA (*c*) for initial scaffold thicknesses of 0.31 mm (white bars) and 0.47 mm (black bars).

the stabilizing lengthening behaviour, although this could also simply be caused by the fact that the scaffold is thicker, therefore leading to lower internal stretches and stresses.

For both the thin and thick constructs, the thickness followed similar trends, first decreasing with culture time up to day 7, after which there was a slight increase in thickness. The initial thinning can be ascribed to the Poisson effect, as the samples are plastically deformed in the in-plane directions. The slight thickening of the samples could be a direct consequence of subsequent tissue formation on top of the scaffold (figure 6), which was also observed by van Vlimmeren *et al.* [51] in statically cultured samples containing the same cells, after four weeks of culture.

Overall, these results indicate that these electrospun polymer materials, often used for tissue-engineering purposes, experience viscoelastic and plastic behaviour, and that different scaffold design parameters can have large implications for reaching a geometrically stable state. This was also reported by Best *et al.* [35] who, by merely increasing the initial lumen diameter in *in situ* TE vascular grafts, could promote enhanced neointimal tissue formation and matched the final size of the lumen to that of the native situation. Similarly, this study demonstrates that the initial thickness of cardiovascular TE grafts can greatly influence the eventual dimensions of these constructs. In this particular case, a geometrical equilibrium state was only found for the thicker samples.

4.2. Mechanical equilibrium at distinctly different magnitudes

For all mechanical constituents, a clear distinction can be observed between the two sample groups (figure 3), which can simply be explained by the differences in initial scaffold thicknesses. For instance, the stretches in both sample groups started at different magnitudes, and slightly increased and decreased for the thin and thick samples, respectively, after which they seemed to reach a steady state. This is particularly odd, since the unloaded construct length continued to dilate in the thinner samples, while it stabilized for the thicker samples. Apparently, the tissue stretch in the thinner sample is maintained at a constant level, although the unloaded state increases over time.

For the thick samples, the Cauchy stresses initially increased, followed by a gradual decrease. An easy explanation can be found in the trend of the sample thickness over time, which appears to be opposite. Contrary, the thinner samples follow a similar trend after day 7, but do not show the initial increase in stress. The temporal changes in tangent stiffness converge to a similar value at the end of the experiment, which gives rise to speculation as to what would happen beyond this time point.

Contrary to earlier findings using this bioreactor system [52], no prestretch was present in any of the tested samples, although histology showed the presence of α-SMA-positive contractile cells (figure 6*g*,*h*). A possible explanation is that in these experiments, a non-degrading scaffold was used, which impairs cell-mediated contraction of the tissue construct, or lies in the fact that these cells predominantly reside in the top layer of the tissue, thus being unable to compact the entire construct.

In these particular experiments, the scaffold seems very important for the mechanical behaviour of the constructs (as is the phase in the initial case for many *in situ* TE applications). In future experiments, it would be very interesting to see what happens to the tissue's mechanical properties if the scaffold is for instance, more compliant or partially degraded [53,54]. Finally, knowing the typical loading pattern in these types of constructs can be very insightful, as this to a great extend determines ECM production and degradation [55–58].

4.3. Tissue composition is similar to the native situation

Although clear differences in mechanical behaviour between the two groups were observed, little differences in tissue composition could be found. Apart from a significant increase in the GAG per number of cells, no significant difference in cell-produced collagen was found. Also no clear differences can be observed qualitatively between the groups (figure 6). Perhaps culture times in these experiments are too short to give rise to such significant differences, or the dominant contribution of the scaffold makes the differences in mechanical behaviour not large enough.

Within the tissue samples themselves, interesting observations can be made. First, a clear top layer is present (figure 6*a*,*b*) containing mainly α-SMA-positive cells, collagen type III and GAGs (figure 6*c*,*d*,*g*,*h*). The presence of the latter three components indicates that this layer is relatively immature, and has probably formed in a later stage of the experiment [51]. Second, on the bottom of the samples thick bundles of collagen type I (figure 6*e*,*f*) and even traces of elastin (figure 6*k*,*l*) are present, implying that this layer

is relatively mature. The existence of these thick bundles of collagen fibres can also be seen in the CNA-stained images (figure 5, left). Noteworthy is the presence of elastin (which appears more abundant in the thinner samples compared to the thick samples), which is rarely observed in similar *in vitro* experiments [59]. Finally, when looking at the gross organization of all the tissue components, they resemble the build-up shown in some *in vivo* TE studies. For instance, we find thick bundles of collagen on the pressurized (bottom) side of our constructs, which coincides with densely organized collagen fibres found in the fibrosa (pressurized) side of native and TE heart valves. In addition, elastin is also found on this side of our samples, which is consistent with a recent study by Kluin *et al.* [13], which also found elastin bundles mainly on the pressurized pulmonary side of TE valve constructs. A possible explanation for these similarities in tissue structure could be attributed to the fact that the loading in the current *in vitro* experiments is very similar to the native situation.

4.4. Comparison to *in vivo* studies

Lengthening of implanted vascular grafts, and subsequent aneurysm formation, has been observed in previous studies [60,61], where a possible explanation lies in the fact that relatively small initial wall thicknesses were used. On the contrary, a recent study by Talacua *et al.* [62] opted for an electrospun PCL scaffold as a vascular graft with a thickness of 0.275 mm, enforced by an additional Gore-tex patch. Over the course of three months, they reported a constant lumen diameter, possible caused by the relatively thick combined PCL and Gore-tex graft. In another study, Kluin *et al.* [13] used a polycarbonate-bisurea valvular graft with a thickness of 0.4 mm, implanted at the pulmonary position in sheep. In analogy with our study, at similar loading pressures (3.3 versus 4 kPa) and comparable initial scaffold thicknesses (0.4 versus 0.47 mm, compared with the thicker group in this study) they also observed a constant tissue length over time. Moreover, the tissue formation in both studies samples is very similar, with elastin and thick collagen bundle formation on the pressurized side of the samples.

4.5. Limitations and future directions

The bioreactor used in this study mimics the pressure loading of (engineered) cardiovascular structures such as heart valves and arteries. For heart valves, this loading regime closely resembles the native situation. However, for arteries an axisymmetric, semi-tubular structure would replicate the construct loading in a more physiological manner. In this particular case, a relatively simple design parameter as scaffold thickness significantly influenced TE construct mechanics and geometrical stability. Naturally, many other scaffold properties are of paramount importance to obtain a mechanical and geometrical stable state, for instance, the effect of scaffold degradation during *in vitro* or *in vivo* experiments. Moreover, cardiovascular tissues tend to exhibit an anisotropic tissue organization, while this study only focused on isotropically organized constructs. A future study should focus on inducing anisotropic loads in the TE constructs, for instance by using an anisotropic scaffold or by altering the bioreactor insert shape. Additionally, different combinations of scaffold mechanical properties and other loading magnitudes could potentially influence experimental outcomes. The culture time of the engineered constructs in our bioreactor is currently limited to 35 days, of which 14 days were static culture to allow for initial tissue development before dynamic culturing. A recent *in vivo* study showed that the lumen diameter of TE arterial grafts increased in the first six months after implantation, yet stabilized after six months [29]. This leaves open the possibility that the geometry of our thin constructs would stabilize beyond the time window used in the current study. However, such long culture times (months to years) are simply not feasible using an *in vitro* set-up. To study the long-term geometrical and mechanical stability of TE cardiovascular substitutes, *in vivo* studies or computational approaches remain the only option.

4.6. Conclusion

In this study, we sought to elucidate if a simple scaffold design parameter such as initial thickness would influence the emergence of a mechanical and geometrical equilibrium state in dynamically cultured *in vitro* TE constructs. A mechanical steady state was reached in both groups, albeit at different magnitudes of the investigated mechanical quantities (elastic stretch, Cauchy stress, strain energy density and tangent stiffness). A stable geometrical situation was only established in the thicker samples, while the thinner constructs continuously elongated. This demonstrates that reaching geometrical and mechanical stability in TE constructs is highly dependent on functional scaffold design.

Data accessibility. All data and numerical code have been stored at SURFdrive, a personal cloud storage service for the Dutch education and research community, and are available upon request.

Authors' contributions. M.v.K., P.O., S.L. and C.B. conceptualized the idea behind this study. M.v.K. and P.O. conducted the experiments and numerical simulations, analyzed the data and wrote the manuscript. W.v.d.B. performed the histological analysis. R.L. was involved in analysing and interpreting the ultrasound data. S.L. and C.B. supervized the project All authors reviewed the manuscript.

Competing interests. We have no competing interests.

Funding. We acknowledge the funding from the European Union's Seventh Framework Programme (grant agreement no. 604514), and the Netherlands Cardiovascular Research Initiative (CVON 2012-01): the Dutch Heart Foundation, Dutch Federation of University Medical Centres, the Netherlands Organization for Health Research and Development, and the Royal Netherlands Academy of Sciences.

Acknowledgements. The authors acknowledge Koo Rijpkema for his advice on the statistical methods, and Wojciech Szymczyk for electrospinning of the scaffolds. In addition, we also acknowledge the ICMS animation studio for designing figure 1.

References

1. O'Hara PJ, Hertzer NR, Beven EG, Krajewski LP. 1986 Surgical-management of infected abdominal aortic grafts: review of a 25-year experience. *J. Vasc. Surg.* **3**, 725–731. (doi:10.1016/0741-5214(86)90036-4)

2. Fernandez G, Costa F, Fontan F, Naftel DC, Blackstone EH, Kirklin JW. 1989 Prevalence of reoperation for pathway obstruction after Fontan

operation. *Ann. Thorac. Surg.* **48**, 654–659. (doi:10.1016/0003-4975(89)90783-2)

3. Suma H. 1999 Arterial grafts in coronary bypass surgery. *Ann. Thorac. Cardiovasc. Surg.* **5**, 141–145.
4. Kannan RY, Salacinski HJ, Butler PE, Hamilton G, Seifalian AM. 2005 Current status of prosthetic bypass grafts: a review. *J. Biomed. Mater. Res.* **74B**, 570–581. (doi:10.1002/jbm.b.30247)
5. Pibarot P, Dumesnil JG. 2009 Prosthetic heart valves: selection of the optimal prosthesis and long-term management. *Circulation* **119**, 1034–1048. (doi:10.1161/CIRCULATIONAHA.108.778886)
6. Ackermann K, Balling G, Eicken A, Guenther T, Schreiber C, Hess J. 2007 Replacement of the systemic atrioventricular valve with a mechanical prosthesis in children aged less than 6 years: late clinical results of survival and subsequent replacement. *J. Thorac. Cardiovasc. Surg.* **134**, 750–756. (doi:10.1016/j.jtcvs.2007.04.025)
7. Lee C, Park CS, Lee CH, Kwak JG, Kim SJ, Shim WS, Song JY, Choi EY, Lee SY. 2011 Durability of bioprosthetic valves in the pulmonary position: long-term follow-up of 181 implants in patients with congenital heart disease. *J. Thorac. Cardiovasc. Surg.* **142**, 351–358. (doi:10.1016/j.jtcvs.2010.12.020)
8. Puvimanasinghe JP, Steyerberg EW, Takkenberg JJ, Eijkemans MJ, van Herwerden LA, Bogers AJ, Habbema JD. 2001 Prognosis after aortic valve replacement with a bioprosthesis: predictions based on meta-analysis and microsimulation. *Circulation* **103**, 1535–1541. (doi:10.1161/01.CIR.103.11.1535)
9. Roh JD *et al.* 2010 Tissue-engineered vascular grafts transform into mature blood vessels via an inflammation-mediated process of vascular remodeling. *Proc. Natl Acad. Sci. USA* **107**, 4669–4674. (doi:10.1073/pnas.0911465107)
10. Dijkman PE, Driessen-Mol A, Frese L, Hoerstrup SP, Baaijens FPT. 2012 Decellularized homologous tissue-engineered heart valves as off-the-shelf alternatives to xeno- and homografts. *Biomaterials* **33**, 4545–4554. (doi:10.1016/j.biomaterials.2012.03.015)
11. Hoerstrup SP *et al.* 2006 Functional growth in tissue-engineered living, vascular grafts: follow-up at 100 weeks in a large animal model. *Circulation* **114**, I159–I166. (doi:10.1161/CIRCULATIONAHA.105.001172)
12. Syedain Z, Reimer J, Lahti M, Berry J, Johnson S, Tranquillo RT. 2016 Tissue engineering of acellular vascular grafts capable of somatic growth in young lambs. *Nat. Commun.* **7**, 12951. (doi:10.1038/ncomms12951)
13. Kluin J *et al.* 2017 *In situ* heart valve tissue engineering using a bioresorbable elastomeric implant: from material design to 12 months follow-up in sheep. *Biomaterials* **125**, 101–117. (doi:10.1016/J.BIOMATERIALS.2017.02.007)
14. Fung YC. 1990 Biomechanical aspects of growth and tissue engineering. In *Biomechanics*, pp. 499–546. New York, NY: Springer.
15. Hoffman BD, Grashoff C, Schwartz MA. 2011 Dynamic molecular processes mediate cellular mechanotransduction. *Nature* **475**, 316–323. (doi:10.1038/nature10316)
16. Humphrey JD. 2008 Vascular adaptation and mechanical homeostasis at tissue, cellular, and sub-cellular levels. *Cell Biochem. Biophys.* **50**, 53–78. (doi:10.1007/s12013-007-9002-3)
17. Humphrey JD, Dufresne ER, Schwartz MA. 2014 Mechanotransduction and extracellular matrix homeostasis. *Nat. Rev. Mol. Cell Biol.* **15**, 802–812. (doi:10.1038/nrm3896)
18. Chaput M, Handschumacher MD, Tournoux F, Hua L, Guerrero JL, Vlahakes GJ, Levine RA. 2008 Mitral leaflet adaptation to ventricular remodeling: occurrence and adequacy in patients with functional mitral regurgitation. *Circulation* **118**, 845–852. (doi:10.1161/CIRCULATIONAHA.107.749440)
19. Oomen PJA, Loerakker S, van Geemen D, Neggers J, Goumans MJTH, van den Bogaerdt AJ, Bogers AJJC, Bouten CVC, Baaijens FPT. 2016 Age-dependent changes of stress and strain in the human heart valve and their relation with collagen remodeling. *Acta Biomater.* **29**, 161–169. (doi:10.1016/j.actbio.2015.10.044)
20. Taber LA, Humphrey JD. 2001 Stress-modulated growth, residual stress, and vascular heterogeneity. *J. Biomech. Eng.* **123**, 528–535. (doi:10.1115/1.1412451)
21. Humphrey JD, Eberth JF, Dye WW, Gleason RL. 2009 Fundamental role of axial stress in compensatory adaptations by arteries. *J. Biomech.* **42**, 1–8. (doi:10.1016/j.jbiomech.2008.11.011)
22. Valentin A, Cardamone L, Baek S, Humphrey JD. 2009 Complementary vasoactivity and matrix remodelling in arterial adaptations to altered flow and pressure. *J. R. Soc. Interface* **6**, 293–306. (doi:10.1098/rsif.2008.0254)
23. Cyron CJ, Humphrey JD. 2014 Vascular homeostasis and the concept of mechanobiological stability. *Int. J. Eng. Sci.* **85**, 203–223. (doi:10.1016/j.ijengsci.2014.08.003)
24. Vigliotti A, Ronan W, Baaijens FPT, Deshpande VS. 2016 A thermodynamically motivated model for stress-fiber reorganization. *Biomech. Model Mechanobiol.* **15**, 761–789. (doi:10.1007/s10237-015-0722-9)
25. Bellini C *et al.* 2017 Comparison of 10 murine models reveals a distinct biomechanical phenotype in thoracic aortic aneurysms. *J. R. Soc. Interface* **14**, 20161036. (doi:10.1098/rsif.2016.1036)
26. Ferruzzi J, Bersi MR, Mecham RP, Ramirez F, Yanagisawa H, Tellides G, Humphrey JD. 2016 Loss of elastic fiber integrity compromises common carotid artery function: implications for vascular aging. *Artery Res.* **14**, 41–52. (doi:10.1016/j.artres.2016.04.001)
27. L'Heureux N *et al.* 2006 Human tissue-engineered blood vessels for adult arterial revascularization. *Nat. Med.* **12**, 361–365. (doi:10.1038/nm1364)
28. McAllister TN *et al.* 2009 Effectiveness of haemodialysis access with an autologous tissue-engineered vascular graft: a multicentre cohort study. *The Lancet* **373**, 1440–1446. (doi:10.1016/S0140-6736(09)60248-8)
29. Khosravi R *et al.* 2016 Long-term functional efficacy of a novel electrospun poly(glycerol sebacate)-based arterial graft in mice. *Ann. Biomed. Eng.* **44**, 2402–2416. (doi:10.1007/s10439-015-1545-7)
30. Schmidt D *et al.* 2010 Minimally-invasive implantation of living tissue engineered heart valves a comprehensive approach from autologous vascular cells to stem cells. *J. Am. Coll. Cardiol.* **56**, 510–520. (doi:10.1016/j.jacc.2010.04.024)
31. Driessen-Mol A *et al.* 2014 Transcatheter implantation of homologous 'off-the-shelf' tissue-engineered heart valves with self-repair capacity: long-term functionality and rapid *in vivo* remodeling in sheep. *J. Am. Coll. Cardiol.* **63**, 1320–1329. (doi:10.1016/j.jacc.2013.09.082)
32. Reimer J, Syedain Z, Haynie B, Lahti M, Berry J, Tranquillo R. 2017 Implantation of a tissue-engineered tubular heart valve in growing lambs. *Ann. Biomed. Eng.* **45**, 439–451. (doi:10.1007/s10439-016-1605-7)
33. Wissing TB, Bonito V, Bouten CVC, Smits AIPM. 2017 Biomaterial-driven *in situ* cardiovascular tissue engineering-a multi-disciplinary perspective. *NPJ Regen. Med.* **2**, 18. (doi:10.1038/s41536-017-0023-2)
34. Miller KS, Khosravi R, Breuer CK, Humphrey JD. 2015 A hypothesis-driven parametric study of effects of polymeric scaffold properties on tissue engineered neovessel formation. *Acta Biomater.* **11**, 283–294. (doi:10.1016/j.actbio.2014.09.046)
35. Best CA *et al.* 2018 Oversized biodegradable arterial grafts promote enhanced neointimal tissue formation. *Tissue Eng. Part A* **24**, 1251–1261. (doi:10.1089/ten.tea.2017.0483)
36. van Kelle MA, Oomen PJ, Bulsink JA, Janssen-van den Broek MW, Lopata RG, Rutten MC, Loerakker S, Bouten CV. 2017 A bioreactor to identify the driving mechanical stimuli of tissue growth and remodeling. *Tissue Eng. Part C Methods* **23**, 377–387. (doi:10.1089/ten.tec.2017.0141)
37. Oomen PJA, van Kelle MAJ, Oomens CWJ, Bouten CVC, Loerakker S. 2017 Nondestructive mechanical characterization of developing biological tissues using inflation testing. *J. Mech. Behav. Biomed. Mater.* **74**, 438–447. (doi:10.1016/j.jmbbm.2017.07.009)
38. Wisse E, Govaert LE, Meijer HEH, Meijer EW. 2006 Unusual tuning of mechanical properties of thermoplastic elastomers using supramolecular fillers. *Macromolecules* **39**, 7425–7432. (doi:10.1021/ma060986i)
39. Neggers J, Hoefnagels JPM, Hild F, Roux S, Geers MGD. 2012 A global digital image correlation enhanced full-field bulge test method. *Procedia IUTAM* **4**, 73–81. (doi:10.1016/j.piutam.2012.05.009)
40. Mol A, Rutten MCM, Driessen NJB, Bouten CVC, Zund G, Baaijens FPT, Hoerstrup SP. 2006 Autologous human tissue-engineered heart valves: prospects for systemic application. *Circulation* **114**, I152–I158. (doi:10.1161/CIRCULATIONAHA.105.001123)

41. Mol A, van Lieshout MI, Veen C, Neuenschwander S, Hoerstrup SP, Baaijens F, Bouten C. 2005 Fibrin as a cell carrier in cardiovascular tissue engineering applications. *Biomaterials* **26**, 3113–3121. (doi:10.1016/j.biomaterials.2004.08.007)
42. Driessen NJB, Mol A, Bouten CVC, Baaijens FPT. 2007 Modeling the mechanics of tissue-engineered human heart valve leaflets. *J. Biomech.* **40**, 325–334. (doi:10.1016/j.jbiomech.2006.01.009)
43. Loerakker S, Argento G, Oomens CWJ, Baaijens FPT. 2013 Effects of valve geometry and tissue anisotropy on the radial stretch and coaptation area of tissue-engineered heart valves. *J. Biomech.* **46**, 1792–1800. (doi:10.1016/j.jbiomech.2013.05.015)
44. Oomen PJA, Holland MA, Bouten CVC, Kuhl E, Loerakker S. 2018 Growth and remodeling play opposing roles during postnatal human heart valve development. *Sci. Rep.* **8**, 1–13. (doi:10.1038/s41598-018-19777-1)
45. Boerboom RA, Krahn KN, Megens RTA, van Zandvoort MAMJ, Merkx M, Bouten CVC. 2007 High resolution imaging of collagen organisation and synthesis using a versatile collagen specific probe. *J. Struct. Biol.* **159**, 392–399. (doi:10.1016/j.jsb.2007.04.008)
46. Frangi AF, Niessen WJ, Vincken KL, Viergever MA. 1998 Multiscale vessel enhancement filtering. In *Medical image computing and computer-assisted intervention - Miccai'98. MICCAI 1998. Lecture notes in computer science* (eds WM Wells, A Colchester, S Delp), vol. 1496, pp. 130–137. Berlin, Germany: Springer.
47. Farndale R, Buttle D, Barret A. 1986 Improved quantitation and discrimination of sulphated glycosaminoglycans by use of dimethylmethylene blue. *Biochim. Biophys. Acta* **883**, 173–177. (doi:10.1016/0304-4165(86)90306-5)
48. Huszar G, Maiocco J, Naftolin F. 1980 Monitoring of collagen and collagen fragments in chromatography of protein mixtures. *Anal. Biochem.* **105**, 424–429. (doi:10.1016/0003-2697(80)90481-9)
49. Cesarone CF, Bolognesi C, Santi L. 1979 Improved microfluorometric DNA determination in biological material using 33258 Hoechst. *Anal. Biochem.* **100**, 188–197. (doi:10.1016/0003-2697(79)90131-3)
50. Duricki DA, Soleman S, Moon LDF. 2016 Analysis of longitudinal data from animals with missing values using SPSS. *Nat. Protoc.* **11**, 1112–1129. (doi:10.1038/nprot.2016.048)
51. van Vlimmeren MAA, Driessen-Mol A, Oomens CWJ, Baaijens FPT. 2013 The potential of prolonged tissue culture to reduce stress generation and retraction in engineered heart valve tissues. *Tissue Eng. Part C Methods* **19**, 205–215. (doi:10.1089/ten.tec.2012.0100)
52. van Kelle MAJ, Oomen PJA, Bulsink JA, Janssen-vandenBroek MWJT, Lopata RGP, Rutten MCM, Loerakker S, Bouten CVC. 2017 A bioreactor to identify the driving mechanical stimuli of tissue growth and remodeling. *Tissue Eng. Part C Methods* **23**, 377–387. (doi:10.1089/ten.TEC.2017.0141)
53. Niklason LE, Gao J, Abbott WM, Hirschi KK, Houser S, Marini R, Langer R. 1999 Functional arteries grown *in vitro*. *Science* **284**, 489–493. (doi:10.1126/science.284.5413.489)
54. Niklason LE, Yeh AT, Calle EA, Bai Y, Valentin A, Humphrey JD. 2010 Enabling tools for engineering collagenous tissues integrating bioreactors, intravital imaging, and biomechanical modeling. *Proc. Natl Acad. Sci. USA* **107**, 3335–3339. (doi:10.1073/pnas.0907813106)
55. Ruberti JW, Hallab NJ. 2005 Strain-controlled enzymatic cleavage of collagen in loaded matrix. *Biochem. Biophys. Res. Commun.* **336**, 483–489. (doi:10.1016/j.bbrc.2005.08.128)
56. Boerboom RA, Rubbens MP, Driessen NJB, Bouten CVC, Baaijens FPT. 2008 Effect of strain magnitude on the tissue properties of engineered cardiovascular constructs. *Ann. Biomed. Eng.* **36**, 244–253. (doi:10.1007/s10439-007-9413-8)
57. Wyatt KEK, Bourne JW, Torzilli Pa. 2009 Deformation-dependent enzyme mechanokinetic cleavage of type I collagen. *J. Biomech. Eng.* **131**, 051004. (doi:10.1115/1.3078177)
58. Humphrey JD, Dufresne ER, Schwartz MA. 2014 Mechanotransduction and extracellular matrix homeostasis. *Nat. Rev. Mol. Cell Biol.* **15**, 802–812. (doi:10.1038/nrm3896)
59. Mol A, Smits AIPM, Bouten CVC, Baaijens FPT. 2009 Tissue engineering of heart valves: advances and current challenges. *Expert Rev. Med. Dev.* **6**, 259–275. (doi:10.1586/ERD.09.12)
60. Khosravi R *et al.* 2016 Long-term functional efficacy of a novel electrospun poly(glycerol sebacate)-based arterial graft in mice. *Ann. Biomed. Eng.* **44**, 2402–2416. (doi:10.1007/s10439-015-1545-7)
61. Ong CS, Zhou X, Huang CY, Fukunishi T, Zhang H, Hibino N. 2017 Tissue engineered vascular grafts: current state of the field. *Expert Rev. Med. Devices* **14**, 383–392. (doi:10.1080/17434440.2017.1324293)
62. Talacua H *et al.* 2015 *In situ* tissue engineering of functional small-diameter blood vessels by host circulating cells only. *Tissue Eng. Part A* **21**, 2583–2594. (doi:10.1089/ten.TEA.2015.0066)